Axisymmetric Instability of Fluid Saturated Pervious Cylinders

J. P. Bardet
Civil Engineering Department,
University of Southern California,
Los Angeles, CA 90089-2531

S. Iai
Geotechnical Earthquake Engineering Laboratory,
Port and Harbour Research Institute,
Yokosuka 239-0826, Japan

The emergence of two-phase instability is investigated analytically for the axisymmetric cylinders made of a pervious solid matrix with pores filled with an interstitial fluid. General analytical solutions are derived for a broad range of constitutive models, and are illustrated for a few specific types of solids. For particular combinations of stresses and material moduli, saturated hypoelastic and elastoplastic solids are found to undergo two-phase instability, whereas their dry solid matrices remain stable. Two-phase instability can emerge within stable single-phase solids due to the interaction between solid matrix and fluid flow. The present analysis provides general analytical solutions useful for investigating the instabilities of axisymmetric soil samples subjected to the undrained triaxial tests of geomechanics. [DOI: 10.1115/1.1505624]

Introduction

Nonlinear pervious solids which have connected pores saturated with an interstitial fluid (i.e., two-phase materials), can become mechanically unstable as shown by Rice [1] for saturated dilatant hardening rocks, and Vardoulakis [2,3] for saturated contractant granular soils. The instabilities of two-phase materials have not been investigated as extensively as those of single-phase solids (e.g., Bardet [4], Biot [5], Chau [6,7], Hill and Hutchinson [8], Vardoulakis [9], and Vardoulakis and Sulem [10]). They have been analyzed using the principle of effective stress (Schrefler et al. [11]) and assuming constant-volume deformations (e.g., Darve [12], Di Prisco and Nova [13], Nova [14], and Lade [15]). These approaches, which consider two-phase materials as single-phase materials, revealed the isochoric instabilities resulting from solid nonlinearities, but neglected the effects of fluid compressibility and fluid flow throughout pervious solids. Bardet and Shiv [16] examined the two-phase instability of plane-strain rectangular samples of pervious solids with voids filled with compressible/incompressible fluids. Bardet [17] showed that two-phase instability causes numerical difficulties for the finite element solutions of plane-strain boundary value problems involving water diffusion within nonlinear solids. So far, two-phase instability has only been investigated for plane-strain problems, and not for axisymmetric conditions, which are very common in soil testing (e.g., Bardet, [18]).

This paper analyzes the two-phase instability of axisymmetric cylinders made of a pervious solid with pores filled with an interstitial fluid. It derives general analytical axisymmetric solutions for a large variety of constitutive models, examines the relations of one and two-phase instabilities, and considers the compressibility of solid and fluid constituents. The present analysis is limited to axisymmetric bifurcation modes, which are commonly observed on cylindrical samples during conventional laboratory experiments. Symmetry-breaking instabilities and antisymmetric bifurcation modes (e.g., lateral buckling and localization of strain within planar shear bands) are beyond the scope of this analysis.

Contributed by the Applied Mechanics Division of THE AMERICAN SOCIETY OF MECHANICAL ENGINEERS for publication in the ASME JOURNAL OF APPLIED MECHANICS. Manuscript received by the ASME Applied Mechanics Division, Apr. 21, 1999; final revision, Sept. 14, 1999. Associate Editor: D. A. Siginer. Discussion on the paper should be addressed to the Editor, Prof. Robert M. McMeeking, Department of Mechanical and Environmental Engineering University of California–Santa Barbara, Santa Barbara, CA 93106-5070, and will be accepted until four months after final publication of the paper itself in the ASME JOURNAL OF APPLIED MECHANICS.

Definitions

Problem Definition. As shown in Fig. 1, the cylinder is made of a pervious solid matrix of height $2H$ and radius R, the pores of which are filled with an interstitial fluid. It is assumed that (1) the fluid is free to permeate through the connected voids of the solid matrix, (2) the lateral side and end extremities of the cylinder are impervious and frictionless, and (3) the specimen remains cylindrical when it is loaded axially in either compression or tension. Hereafter, the solid-fluid mixture is referred to as a two-phase material. The geometry of Fig. 1 is intended to represent that of soil samples subjected to the undrained triaxial testing in soil mechanics (e.g., Bardet [18]). In these tests, cylindrical soil samples are saturated with water, compressed axially through lubricated frictionless platens, and confined laterally with pressure. Similar geometries are also found in the testing of other porous solids (e.g., rocks and concrete). The boundary conditions are carefully selected so that the fluid pressure, stress, and strain can be assumed uniform and axisymmetric throughout the cylinder. At any given loading state, the Cauchy stress components anywhere within the cylinder are

$$\sigma_{rr}=\sigma_{\theta\theta} \quad \text{and} \quad \sigma_{rz}=\sigma_{r\theta}=\sigma_{z\theta}=0 \tag{1}$$

where σ_{rr}, $\sigma_{\theta\theta}$, $\sigma_{r\theta}$, σ_{rz}, and $\sigma_{z\theta}$ are the Cauchy stress components in the polar coordinates r, θ, and z of Fig. 1.

Possible departures from uniform states will be investigated by formulating a linear stability (or incremental bifurcation) problem. Starting from a given uniform state of fluid pressure, stress, and strain, we investigate the circumstances for which the rates of fluid pressure, solid stresses, and solid strains may become nonuniform within the cylinder. For a given rate of prescribed loading, the boundary conditions of the incremental bifurcation problem are as follows:

$$v_z=0, \quad \dot{t}_{rz}=0 \quad \text{and} \quad \dot{p}_{,z}=0 \quad \text{for } z=\pm H \quad \text{and} \quad 0\leqslant r\leqslant R \tag{2a}$$

$$v_r=0, \quad \dot{t}_{rz}=0 \quad \text{and} \quad \dot{p}_{,r}=0 \quad \text{for } r=R \quad \text{and} \quad -H\leqslant z\leqslant H \tag{2b}$$

where $\dot{p}$ is the time rate of fluid pressure change, $\mathbf{v}$ the solid velocity, and $\dot{\mathbf{t}}$ the rate of applied distributed force at the boundary. The partial differentiation with respect to r, θ, and z are denoted with "$,r$" "$,\theta$", and "$,z$" and the derivative with respect to time with a dot. The incremental bifurcation problem will now be completed by introducing geometric and material nonlinearities, and equilibrium equations.

Stress States and Rates. By definition, the distributed force vector $\mathbf{t}$ acting on the deformed surface, with area dS_t and unit

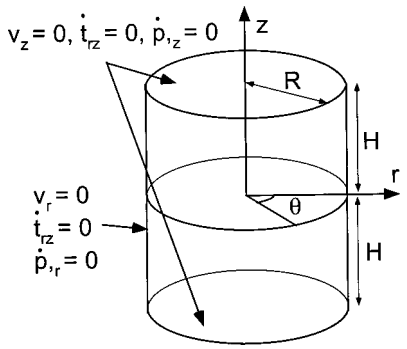

Fig. 1 Geometry, coordinate systems, and boundary conditions of cylindrical porous solid for linear stability analysis

normal vector **n**, is related to the Cauchy stress tensor σ and the nominal (Piola-Kirchhoff) stress tensor Σ through

$$\mathbf{t}=\mathbf{n}\cdot\sigma dS_t=\mathbf{N}\cdot\Sigma dS_o \tag{3}$$

where **N** and dS_o are the unit normal vector and area, respectively, of the reference surface. Nominal and Cauchy stresses are related through

$$\Sigma=\det(\mathbf{F})\mathbf{F}^{-1}\cdot\sigma \tag{4}$$

where $\mathbf{F}^{-1}$ is the inverse transformation of the deformation gradient **F**. By definition the Kirchhoff stress tensor τ is related to σ through

$$\tau=\det(\mathbf{F})\sigma \tag{5}$$

The rates of **t** and Σ are

$$\dot{\mathbf{t}}=\mathbf{N}\cdot\dot{\Sigma}dS_o \quad \text{and} \quad \dot{\Sigma}=\det(\mathbf{F})\mathbf{F}^{-1}\cdot(\dot{\sigma}-\mathbf{L}\cdot\sigma+\sigma\,\mathrm{trace}(\mathbf{L})) \tag{6}$$

where **L** is the velocity gradient tensor.

Rate-Type Constitutive Models. In the present linear stability analysis, the behavior of the solid materials is modeled with rate-type equations (Truesdell and Noll [19])

$$\hat{\tau}=\mathbf{C}\cdot\mathbf{D} \tag{7}$$

where $\hat{\tau}$ is the Jaumann rate of Kirchhoff stress τ, **D** the rate of deformation, and **C** the fourth-order stiffness tensor. In general, **C** is homogeneous of degree zero in **D** and depends on the states of stress and strain. The Jaumann rate of Kirchhoff stress is

$$\hat{\tau}=\dot{\tau}-\mathbf{W}\cdot\tau+\tau\cdot\mathbf{W}. \tag{8}$$

The rate of deformation **D** and spin tensor **W** are

$$\mathbf{D}=\tfrac{1}{2}(\mathbf{L}+\mathbf{L}^T) \quad \mathbf{W}=\tfrac{1}{2}(\mathbf{L}-\mathbf{L}^T) \tag{9}$$

where the superscript "^{T}" denotes transpose. The Jaumann rate of Cauchy stress $\hat{\sigma}$, which is defined similarly to Eq. (8), is related to $\hat{\tau}$ through

$$\hat{\tau}=\det(\mathbf{F})(\hat{\sigma}+\sigma\,\mathrm{trace}(\mathbf{D})). \tag{10}$$

When the present configuration is chosen as reference, the deformation gradient is approximately equal to the unity transformation **1**:

$$\mathbf{F}\approx\mathbf{F}^{-1}\approx\mathbf{1} \quad \text{and} \quad \det(\mathbf{F})\approx 1. \tag{11}$$

In this condition, the nominal, Cauchy, and Kirchhoff stress tensors are identical:

$$\Sigma=\sigma=\tau \tag{12}$$

and their rates are related through

$$\hat{\tau}=\hat{\sigma}+\sigma\,\mathrm{trace}(\mathbf{D}) \quad \text{and} \quad \dot{\Sigma}=\hat{\sigma}+\sigma\,\mathrm{trace}(\mathbf{D})-\sigma\cdot\mathbf{W}-\mathbf{D}\cdot\sigma. \tag{13}$$

The generality of the present analysis is not affected by the choice of the Jaumann rate of Kirchhoff stress. As shown in Bardet [4], the analysis applies to other types of objective stress rates after adding stress-dependent moduli to the constitutive moduli in Equation (7).

Axisymmetric Conditions. In the case of axisymmetric velocity fields (i.e., $v_\theta=0$ and $v_{r,\theta}=v_{z,\theta}=0$), the nonzero terms of deformation rate and spin tensors are

$$D_{rr}=v_{r,r}, \quad D_{zz}=v_{z,z}, \quad D_{\theta\theta}=\frac{v_r}{r},$$

$$D_{rz}=\tfrac{1}{2}(v_{r,z}+v_{z,r}), \quad W_{rz}=-W_{zr}=\tfrac{1}{2}(v_{r,z}-v_{z,r}). \tag{14}$$

Hereafter, we consider the following axisymmetric constitutive equation:

$$\hat{\tau}_{rr}=C_{11}D_{rr}+C_{12}D_{\theta\theta}+C_{13}D_{zz} \tag{15a}$$

$$\hat{\tau}_{\theta\theta}=C_{12}D_{rr}+C_{11}D_{\theta\theta}+C_{13}D_{zz} \tag{15b}$$

$$\hat{\tau}_{zz}=C_{31}D_{rr}+C_{31}D_{\theta\theta}+C_{33}D_{zz} \tag{15c}$$

$$\hat{\tau}_{rz}=2C_{44}D_{rz} \tag{15d}$$

where C_{11}, C_{12}, C_{13}, C_{33}, C_{31}, and C_{44} are constitutive moduli. This general constitutive form, which was used by Chau [6,7] will be later specified for some particular types of constitutive models.

Equilibrium Equations. In axisymmetric conditions and cylindrical coordinates, the stress-rate equilibrium equations for solid materials are (Hill [20]):

$$\dot{\Sigma}_{rr,r}+\dot{\Sigma}_{zr,z}+\frac{1}{r}(\dot{\Sigma}_{rr}-\dot{\Sigma}_{\theta\theta})=0$$

$$\dot{\Sigma}_{rz,r}+\dot{\Sigma}_{zz,z}+\frac{1}{r}\dot{\Sigma}_{rz}=0. \tag{16}$$

Using Eq. (13), Eq. (16) can be expressed in terms of Cauchy stress:

$$\hat{\sigma}_{rr,r}+\hat{\sigma}_{zr,z}+\frac{1}{r}(\hat{\sigma}_{rr}-\hat{\sigma}_{\theta\theta})+(\sigma_{rr}-\sigma_{zz})W_{zr,z}=0 \tag{17a}$$

$$\hat{\sigma}_{rz,r}+\hat{\sigma}_{zz,z}+\frac{1}{r}\hat{\sigma}_{rz}+(\sigma_{rr}-\sigma_{zz})\left(W_{zr,r}+\frac{1}{r}W_{zr}\right)=0. \tag{17b}$$

Solid-Fluid Coupling. The solid-fluid coupling is described using the following generalized effective stress principle (Schrefler et al. [11]):

$$\sigma'_{ij}=\sigma_{ij}+\alpha p\,\delta_{ij} \tag{18}$$

where σ_{ij} is the total Cauchy stress tensor, σ'_{ij} the effective Cauchy stress tensor, and p the interstitial fluid pressure. By sign convention, both σ_{ij} and σ'_{ij} are positive in tension, and p is positive in compression. The coefficient α is a positive constant that depends on the bulk modulus K of the solid skeleton and the bulk modulus K_s of the solid grains as (Schrefler et al. [11])

$$\alpha=1-K/K_s. \tag{19}$$

The physical parameter α is mathematically convenient to model the solid-fluid coupling from complete (i.e., $\alpha=1$) to none (i.e., $\alpha=0$). Hereafter, the superscript prime is omitted for effective stress because all stresses for the solid phase are effective. By substituting Eq. (18) into Eq. (17), the axisymmetric equilibrium equations for two-phase materials are

$$\hat{\sigma}_{rr,r}+\hat{\sigma}_{zr,z}+\frac{1}{r}(\hat{\sigma}_{rr}-\hat{\sigma}_{\theta\theta})+(\sigma_{rr}-\sigma_{zz})W_{zr,z}=\alpha\dot{p}_{,r} \tag{20a}$$

$$\hat{\sigma}_{rz,r}+\hat{\sigma}_{zz,z}+\frac{1}{r}\hat{\sigma}_{rz}+(\sigma_{rr}-\sigma_{zz})\left(W_{zr,r}+\frac{1}{r}W_{zr}\right)=\alpha\dot{p}_{,z}. \tag{20b}$$

The fluid pressure p obeys the flow conservation equation (Schrefler et al. [11])

$$p_{,rr}+\frac{1}{r}p_{,r}+p_{,zz}=\beta\left[\alpha\left(v_{r,r}+\frac{1}{r}v_r+v_{z,z}\right)+\frac{\dot{p}}{\Theta}\right] \tag{21}$$

where the parameter β is related to the fluid unit weight γ_w and coefficient of permeability k through

$$\beta=\gamma_w/k. \tag{22}$$

The parameter Θ is the bulk modulus of the two-phase material, which is related to the porosity n and the fluid bulk modulus K_f as follows (Schrefler et al. [11]):

$$\frac{1}{\Theta}=\frac{n}{K_f}+\frac{\alpha-n}{K_s}. \tag{23}$$

After introducing the following coefficients

$$d_1=C_{11}-\sigma_{rr},\quad d_2=C_{33}-\sigma_{zz} \tag{24a}$$

$$d_3=C_{44}-\tfrac{1}{2}(\sigma_{rr}-\sigma_{zz}),\quad d_4=C_{44}+C_{13}+\tfrac{1}{2}(\sigma_{rr}+\sigma_{zz}) \tag{24b}$$

$$d_5=C_{44}+\tfrac{1}{2}(\sigma_{rr}-\sigma_{zz}),\quad d_6=C_{44}+C_{31}-\tfrac{1}{2}(\sigma_{rr}+\sigma_{zz}) \tag{24c}$$

Eqs. (20) and (21) become

$$d_1\left(v_{r,rr}+\frac{1}{r}v_{r,r}-\frac{1}{r^2}v_r\right)+d_3v_{r,zz}+d_4v_{z,rz}=\alpha\dot{p}_{,r} \tag{25a}$$

$$d_5\left(v_{z,rr}+\frac{1}{r}v_{z,r}\right)+d_2v_{z,zz}+d_6\left(v_{r,rz}+\frac{1}{r}v_{r,z}\right)=\alpha\dot{p}_{,z} \tag{25b}$$

$$\dot{p}_{,rr}+\frac{1}{r}\dot{p}_{,r}+\dot{p}_{,zz}=\beta\left[\alpha\left(\dot{v}_{r,r}+\frac{1}{r}\dot{v}_r+\dot{v}_{z,z}\right)+\frac{\ddot{p}}{\Theta}\right]. \tag{25c}$$

Equation (25) is independent of C_{12} due to axisymmetric conditions. The incremental boundary value problem is finally formulated in terms of solid velocity v_r and v_z and fluid pressure p after restating Eq. (2) as follows:

$$v_z=0,\quad v_{z,r}=0,\quad v_{r,z}=0\quad\text{and}\quad\dot{p}_{,z}=0\quad\text{for}\quad z=\pm H\quad\text{and}\quad 0\leqslant r\leqslant R \tag{26a}$$

$$v_r=0,\quad v_{z,r}=0,\quad v_{r,z}=0\quad\text{and}\quad\dot{p}_{,r}=0\quad\text{for}\quad r=R\quad\text{and}\quad -H\leqslant z\leqslant H. \tag{26b}$$

Trivial and Nontrivial Bifurcating Solutions. Fields of constant solid velocity gradient and fluid pressure are obvious solutions of Eqs. (25) and (26). The nontrivial bifurcating solutions are sought in the following modes:

$$v_r=V_1J_1(\beta_1r)\cos(\beta_2z+\theta_2)f(t) \tag{27a}$$

$$v_z=V_2J_0(\beta_1r)\sin(\beta_2z+\theta_2)f(t) \tag{27b}$$

$$\dot{p}=PJ_0(\beta_1r)\cos(\beta_2z+\theta_2)f(t) \tag{27c}$$

where $J_n(x)$ is the Bessel function of the first kind and nth order, and θ_2 denotes a phase shift. These modes satisfy the boundary conditions of Eq. (26) when β_1, β_2, and θ_2 are selected as follows:

$$\beta_1R=0,\quad\pm3.832,\quad\pm7.016,\quad\pm10.173,\ldots(\text{roots of } J_1=0) \tag{28a}$$

$$\beta_2H=\frac{\pi}{2}m_2\quad\text{for } m_2\text{ integer} \tag{28b}$$

$$\theta_2=\begin{cases}0 & (\text{for } m_2 \text{ even})\\ \dfrac{\pi}{2} & (\text{for } m_2 \text{ odd})\end{cases}. \tag{28c}$$

By substituting these modes into Eq. (25) and introducing f^* so that

$$f^*=\beta\frac{\dot{f}(t)}{f(t)}, \tag{29}$$

the following relations are obtained:

$$\begin{bmatrix}\beta_1^2d_1+\beta_2^2d_3 & \beta_1\beta_2d_4 & -\alpha\beta_1\\ \beta_1\beta_2d_6 & \beta_1^2d_5+\beta_2^2d_2 & -\alpha\beta_2\\ \alpha\beta_1f^* & \alpha\beta_2f^* & \beta_1^2+\beta_2^2+\dfrac{f^*}{\Theta}\end{bmatrix}\begin{Bmatrix}V_1\\V_2\\P\end{Bmatrix}=\begin{Bmatrix}0\\0\\0\end{Bmatrix}. \tag{30}$$

From the third line in Eq. (30), f^* is given by

$$f^*=\frac{-(\beta_1^2+\beta_2^2)P}{\alpha(\beta_1V_1+\beta_2V_2)+\dfrac{P}{\Theta}}. \tag{31}$$

The coefficient f^* is thus independent of time and space and, hence, the solution of Eq. (29) is

$$f(t)=f_0\exp(f^*t/\beta) \tag{32}$$

where f_0 represents an initial amplitude of the nontrivial bifurcating solution. When $f^*>0$, $f(t)$ grows exponentially with time and eventually becomes infinite. Hence, the bifurcating solution generates a material instability. When $f^*\leqslant0$, the bifurcating solution dies out with time, and has little physical relevance. A set of nontrivial bifurcating solutions for V_1, V_2, and P exist when the determinant of the matrix in Eq. (30) becomes zero. After defining the wavelength ratio of the bifurcating mode as

$$\Lambda=\frac{\beta_2}{\beta_1}, \tag{33}$$

the condition for the existence of nontrivial bifurcating solutions in Eq. (30) is

$$\frac{\alpha^2f^*}{\beta_1^2+\beta_2^2}=\frac{N(\Lambda)}{D(\Lambda)}>0. \tag{34}$$

The numerator and denominator of the left side of Eq. (34) are

$$N(\Lambda)=a_1\Lambda^4+b_1\Lambda^2+c_1,\quad D(\Lambda)=a_2\Lambda^4+b_2\Lambda^2+c_2 \tag{35}$$

where

$$a_1=d_2d_3,\quad b_1=d_1d_2+d_3d_5-d_4d_6,\quad c_1=d_1d_5 \tag{36a}$$

$$a_2=-d_3-a_1\chi,\quad b_2=-d_1-d_2+d_4+d_6-b_1\chi,\quad c_2=-d_5-c_1\chi \tag{36b}$$

$$\chi=1/\alpha^2\Theta. \tag{36c}$$

Three types of instability and associated conditions can be defined:

$$\text{solid-fluid } (SF) \text{ instability for } N(\Lambda)/D(\Lambda)>0 \tag{37a}$$

$$\text{infinite solid-fluid } (SF\infty) \text{ instability for } D(\Lambda)=0\quad\text{and}\quad N(\Lambda)\neq0 \tag{37b}$$

$$\text{solid } (S) \text{ instability for } N(\Lambda)=0 \tag{37c}$$

The SF instability is obtained when there are modes with wavelength ratios Λ satisfying Eq. (37*a*). The $SF\infty$ instability is a particular SF instability with $f^*\to+\infty$, which corresponds to an

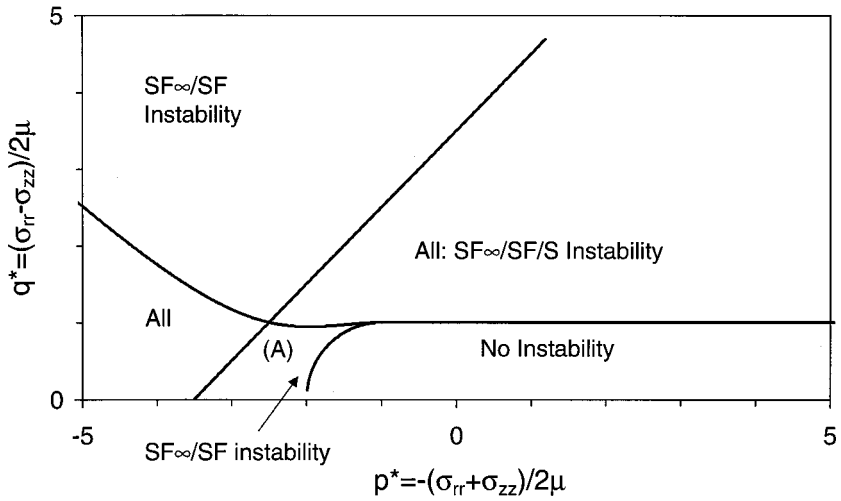

Fig. 2 Dimensionless p^*-q^* domains of *S*, *SF*, and *SF*∞ instabilities for hypoelastic material with incompressible fluid ($\chi^*=0$, $\nu=0.3$)

infinite exponential growth, and a severe solid-fluid instability. The *S* instability is the material instability obtained for the solid alone without interstitial water. The *S* instability is obtained by setting $\alpha=0$ in Eq. (30), fully decoupling the solid and fluid, and ignoring the interstitial fluid. *SF* instability can be physically interpreted as the result of a rapidly growing flow of interstitial fluid through the pervious solid, which may create solid-fluid interaction forces and promote the emergence of nonuniform modes of deformation. In theory, *SF* instability could be detected by measuring the spatial fluctuation of fluid pressure within the material specimens tested in the laboratory.

Applications

The one and two-phase axisymmetric instabilities will be examined for three particular types of rate-type constitutive equations: (1) hypoelastic models, (2) elastoplastic models, and (3) Rudnicki pressure-sensitive models.

Hypoelastic Model. The constitutive moduli of isotropic hypoelastic models are (Bardet [4])

$$C_{11}=C_{33}=2\mu+\lambda, \quad C_{13}=C_{31}=\lambda \quad \text{and} \quad C_{44}=\mu \tag{38}$$

where μ is the shear modulus and λ the Lame's modulus, which are related to Poisson's ratio ν through

$$\lambda=\frac{2\nu\mu}{1-2\nu}. \tag{39}$$

It is convenient to introduce the following nondimensional stress components and coefficients:

$$p^*=-\frac{\sigma_{rr}+\sigma_{zz}}{2\mu} \quad q^*=\frac{\sigma_{rr}-\sigma_{zz}}{2\mu}, \quad \text{and} \quad \chi^*=\mu\chi. \tag{40}$$

The hypoelastic model is useful for developing closed-form analytical solutions for simple linear stability problems and comparing numerical and analytical results (e.g., Bardet [17]). However, the hypoelastic model has only two material parameters, and therefore limited capabilities in modeling realistically all types of material responses.

Figures 2 to 4 show the p^*-q^* domains of *S*, *SF*, and *SF*∞ instability for various cases of fluid and solid compressibility. By definition, p^* is positive in compression and negative in tension. These p^*-q^* domains are symmetric about the p^*- axis, and are

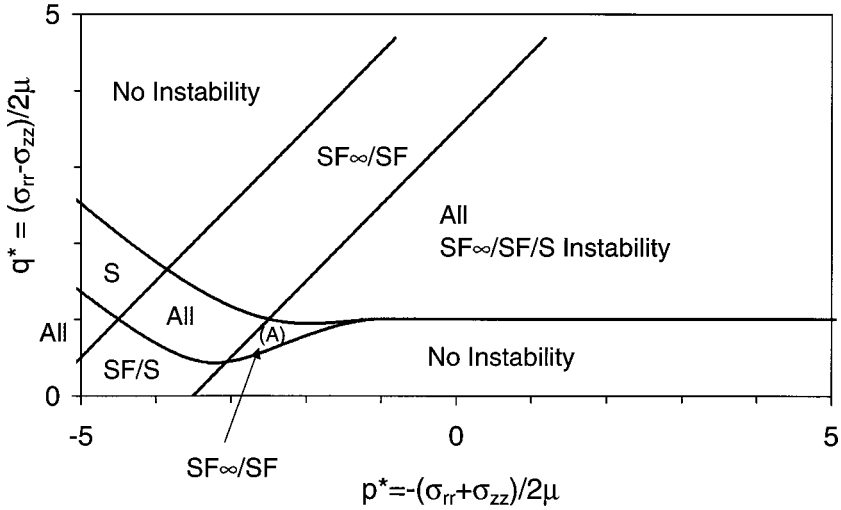

Fig. 3 Dimensionless p^*-q^* domains of *S*, *SF*, and *SF*∞ instabilities for hypoelastic material with compressible fluid ($\chi^*=0.5$, $\nu=0.3$)

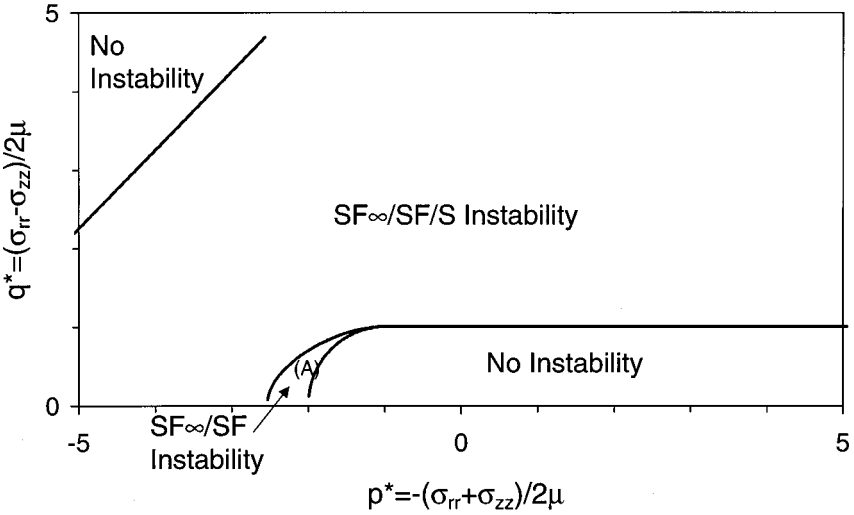

Fig. 4 Dimensionless p^*-q^* domains of *S*, *SF*, and *SF*∞ instabilities for hypoelastic material with compressible fluid ($\chi^*=0.5$, $\nu=0.43$)

only represented for positive values of q^*. As shown in Fig. 2 for incompressible fluid (i.e., $\chi^*=0$), zero stress states are initially stable. For $q^*=1$ and $p^*>0$, all types of instability emerge simultaneously. For $p^*<-2$, *SF* and *SF*∞ instabilities appear in area *A* without *S* instability. As shown in Fig. 3, the size of area A shrinks with the compressibility of the interstitial fluid (i.e., $\chi^*=0.5$). *SF* and *S* instabilities may occur simultaneously when p^* decreases below 3. As shown in Fig. 4, the size of area A also shrinks as the solid becomes more incompressible (i.e., $\nu=0.43$), and vanishes for incompressible material (i.e., $\nu=0.5$). In the incompressible limit, *S*, *SF*, and *SF*∞ instabilities may emerge simultaneously.

Elastoplastic Mohr-Coulomb Model. The constitutive moduli of elastoplasticity are (Hill [21] and Bardet [4])

$$C_{11}=2\mu+\lambda-\frac{1}{H'}[2\mu P_{11}+\lambda(P_{33}+2P_{11})]\times[2\mu Q_{11}+\lambda(Q_{33}+2Q_{11})],$$

$$C_{33}=2\mu+\lambda-\frac{1}{H'}[2\mu P_{33}+\lambda(P_{33}+2P_{11})]\times[2\mu Q_{33}+\lambda(Q_{33}+2Q_{11})],$$

$$C_{13}=\lambda-\frac{1}{H'}[2\mu P_{11}+\lambda(P_{33}+2P_{11})][2\mu Q_{33}+\lambda(Q_{33}+2Q_{11})],$$

$$C_{31}=\lambda-\frac{1}{H'}[2\mu P_{33}+\lambda(P_{33}+2P_{11})][2\mu Q_{11}+\lambda(Q_{33}+2Q_{11})],$$

$$C_{44}=\mu$$

$$H'=H+\lambda(P_{33}+2P_{11})(P_{33}+2P_{11})+2\mu(2P_{11}Q_{11}+P_{33}Q_{33}) \tag{41}$$

where H is the plastic modulus; and P_{ij} and Q_{ij} are unit tensors representing the flow and yield directions, respectively. For a Mohr-Coulomb material and axisymmetric conditions, the unit tensors P_{ij} and Q_{ij} are related to the mobilized friction angle ϕ and the dilatancy angle ψ as follows:

$$P_{33}=\frac{\sin\psi-2}{\sqrt{3(2+\sin^2\psi)}} \quad \text{and} \quad P_{11}=\frac{1+\sin\psi}{\sqrt{3(2+\sin^2\psi)}} \tag{42a}$$

$$Q_{33}=\frac{-2(1-\sin\phi)}{\sqrt{2(3-2\sin\phi+3\sin^2\phi)}} \quad \text{and}$$

$$Q_{11}=\frac{1+\sin\phi}{\sqrt{2(3-2\sin\phi+3\sin^2\phi)}} \tag{42b}$$

where the mobilized friction angle φ and the dilatancy angle ψ are defined by

$$\sin\phi=\left|\frac{\sigma_{zz}-\sigma_{rr}}{\sigma_{zz}+\sigma_{rr}}\right| \quad \text{and}$$

$$\sin\psi=\frac{-(d\varepsilon^p_{zz}+2d\varepsilon^p_{rr})}{d\varepsilon^p_{zz}-d\varepsilon^p_{rr}}=\frac{-(P_{33}+2P_{11})}{P_{33}-P_{11}}. \tag{43}$$

Figure 5 shows an example of instability domain in the $\phi-H/\mu$ plane for $\nu=0.3$, $\psi=-30$ deg and $\chi^*=0$. The variations of elastoplastic moduli for fixed values of ν, ψ, and χ^* are characterized solely by the values of ϕ and H/μ, which are represented using the point M of coordinates $\phi-H/\mu$ in Fig. 5. When the stress states are initially isotropic at the beginning of a shear loading, the point M is initially in the upper left corner, which corresponds to an elastic state ($H\gg1$) and no shear stress ($\phi=0$). As the shear stress increases, point M moves down from the upper left corner and intersects the SF/S boundary, or *SF*∞/*SF* boundary. If $\phi<8$ deg, point M intersects first the *SF/S* boundary for strain-softening conditions ($H<0$). In this case, *SF* and *S* instabilities will occur simultaneously. If $\phi>8$ deg, point M will intersect the *SF*∞/*SF* boundary for either strain-softening, strain-hardening ($H>0$), or perfectly plastic ($H=0$) conditions. This implies that *SF*∞ and/or *SF* instabilities may emerge without *S* instabilities for contractant elastoplastic materials. In other words, *SF*∞ and/or *SF* instabilities are not necessarily generated by *S* instabilities.

Rudnicki Model. In the investigation of material instability, Rudnicki [22] proposed the following rate-independent constitutive model for axisymmetric conditions, which generalizes most constitutive models used in linear stability analyses

$$C_{11}=9K/4+G_t, \quad C_{13}=9K\nu/2, \quad C_{31}=9Kr^*/4,$$

$$C_{33}=E/2+9K\nu r^*/2, \quad C_{44}=G_l, \tag{44}$$

where K, E, ν, r^*, G_l, and G_t are material moduli, the physical meanings of which are defined in Rudnicki [22] and Chau [7].

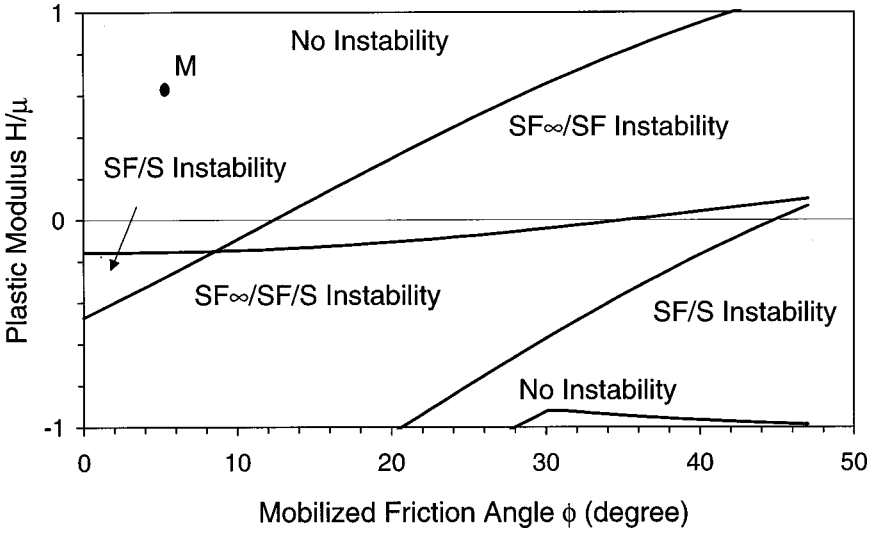

Fig. 5 Domain of *S*, *SF*, and *SF*∞ instabilities for elastoplastic contractant Mohr-Coulomb material and incompressible fluid (ν=0.3, ψ=−30 deg and χ^*=0)

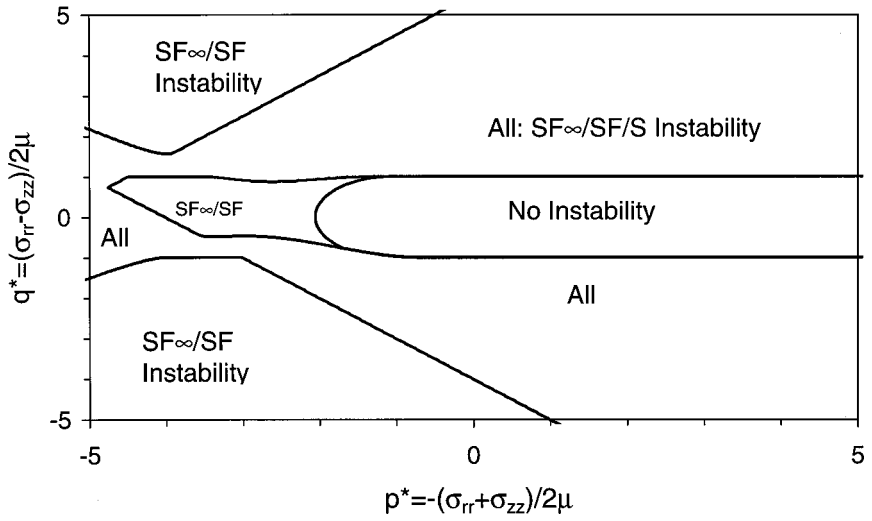

Fig. 6 Dimensionless *p-*q** domains of *S*, *SF*, and *SF*∞ instabilities for Rudnicki's model for incompressible fluid (χ^*=0, $G_l/2G_t$=0.5, $K/2G_t$=1, ν=0.3, and r^*=0.6)**

Figure 6 shows the domains of instability of Ruckniki's model in the p^*-q^* coordinates used for the hypoelastic model of Figs. 2–4 for particular values of material parameters: $G_l/2G_t=0.5$; $K/2G_t=1$; $\nu=0.3$; $r^*=0.6$; and incompressible interstitial fluid $\chi^*=0$. For this particular selection of model parameters, the domains of *S*, *SF*, and *SF*∞ instabilities are similar to those of Fig. 2, except for the asymmetry about the q^*-axis. As for hypoelastic models, *SF* and *SF*∞ instabilities are not generated by *S* instability in area A.

Discussion

A general mathematical framework and analytical solutions have been derived for studying the two-phase instability of axisymmetric cylinders made of a wide variety of pervious solids filled with a compressible/incompressible fluid. The present analysis is based on the assumptions stated in Eqs. (17), (18), and (21). The analysis holds provided that these mechanical assumptions represent the material physics, but may break down in some circumstances, e.g., when Eqs. (18) and (21) do not hold due to capillary effects and bubble formation in the interstitial fluid (Schrefler et al. [11]).

The analysis needs to be extended to nonaxisymmetric deformations (e.g., strain localization), which have been shown in the case of dry solids to become the predominant modes of instability when the axisymmetry constraints are removed (e.g., Chau [7,23]). The general framework and solutions also need to be applied to constitutive models specific to geomechanics and investigated in the context of undrained triaxial testing. There is also a need to investigate the effects of two-phase instability on the numerical solutions of liquefaction problems in geomechanics, following the approach of Bardet [17] for hypoelastic materials.

Conclusions

The emergence of two-phase instability was investigated analytically in the case of pervious solid cylinders with voids filled with an interstitial fluid. The analysis develops a mathematical framework and analytical solutions that apply to a broad range of

material models, and illustrates their application for specific types of solids including hypoelastic and elastoplastic models. For particular values of stress states and material moduli, hypoelastic and elastoplastic models were found to undergo two-phase instability, and no solid instability. Two-phase instability can emerge in stable solids due to the interaction between fluid flow and porous solid matrix. The general results of the present analysis are relevant to geomechanics for studying instabilities in undrained triaxial tests.

Acknowledgment

The authors acknowledge the financial support of the U.S. National Science Foundation and the Science and Technology Agency, Japan.

References

[1] Rice, J. R., 1975, ''On the Stability of Dilatant Hardening of Saturated Rock Masses,'' J. Geophys. Res., **80**, pp. 1531–1536.
[2] Vardoulakis, I., 1985, ''Stability and Bifurcation of Undrained, Plane Rectilinear Deformation on Water-Saturated Granular Soils,'' Int. J. Numer. Analyt. Meth. Geomech., **9**, pp. 399–414.
[3] Vardoulakis, I., 1986, ''Dynamic Stability Analysis of Undrained Simple Shear on Water-Saturated Granular Soils,'' Int. J. Numer. Analyt. Meth. Geomech., **10**, pp. 177–190.
[4] Bardet, J. P., 1991, ''Analytical Solutions for the Plane Strain Bifurcation of compressible solids,'' ASME J. Appl. Mech., **58**, pp. 651–657.
[5] Biot, M. A., 1965, *Mechanics of Incremental Deformation*, John Wiley and Sons, New York.
[6] Chau, K. T., 1992, ''Non-normality and Bifurcation in a Compressible Pressure-Sensitive Circular Cylinder Under Axisymmetric Tension and Compression,'' Int. J. Solids Struct., **29**, pp. 801–824.
[7] Chau, K. T., 1993, ''Antisymmetric Bifurcations in a Compressible Pressure-Sensitive Circular Cylinder Under Axisymmetric Tension and Compression,'' ASME J. Appl. Mech., **60**, pp. 282–289.
[8] Hill, R., and Hutchinson, J. W., 1975, ''Bifurcation Phenomena in the Plane Tension Test,'' J. Mech. Phys. Solids, **23**, pp. 239–264.
[9] Vardoulakis, I., 1981, ''Bifurcation Analysis of the Plane Rectilinear Deformation on Dry Sand Samples,'' Int. J. Solids Struct., **17**(11), pp. 1085–1101.
[10] Vardoulakis, I., and Sulem, J., 1995, *Bifurcation Analysis in Geomechanics*, Blackie Academic & Professional, Glasgow, UK, p. 459.
[11] Schrefler, B. A., Simoni, L., Xikui, L., and Zienkiewicz, O. C., 1990, ''Mechanics of Partially Saturated Porous Media,'' *Numerical Methods and Constitutive Modeling in Geomechanics*, C. S. Desai and G. Gioda, eds., Springer-Verlag, New York, pp. 169–209.
[12] Darve, F., 1994, ''Stability and Uniqueness in Geomaterials Constitutive Modeling,'' *Localization and Bifurcation Theory for Soils and Rocks*, R. Chambon, J. Desrues, and I. Vardoulakis, eds., A. A. Balkema, Rotterdam, The Netherlands, pp. 73–88.
[13] Di Prisco, C., and Nova, R., 1994, ''Stability Problems Related to Static Liquefaction of Loose Sand,'' *Localization and Bifurcation Theory for Soils and Rocks*, R. Chambon, J. Desrues, and I. Vardoulakis, eds., A. A. Balkema, Rotterdam, The Netherlands, pp. 59–70.
[14] Nova, R., 1991, ''A Note on Sand Liquefaction and Soil Stability,'' *Constitutive Laws for Engineering Materials*, C. S. Desai et al., ASME, New York, pp. 153–156.
[15] Lade, P. V., 1989, ''Experimental Observations of Stability, Instability and Shear Planes in Granular Materials,'' Ingenieur-Archiv, **59**, pp. 114–123.
[16] Bardet, J. P., and Shiv, A., 1995, ''Plane-Strain Instability of Saturated Porous Media,'' J. Eng. Mech. **121**(6), pp. 717–724.
[17] Bardet, J. P., 1996, ''Finite Element Analysis of Two-Phase Instability for Saturated Porous Hypoelastic Solids Under Plane Strain Loadings,'' Eng. Comput., **13**(7), pp. 29–48.
[18] Bardet, J. P., 1997, *Experimental Soil Mechanics*, Prentice-Hall, Englewood Cliffs, NJ.
[19] Truesdell, C., and Noll, W., 1965 *Nonlinear Field Theories of Mechanics* (Handbuch of Physics III/3), Springer-Verlag, Berlin.
[20] Hill, R., 1959, ''Some Basic Principles in the Mechanics of Solids Without a Natural Time,'' J. Mech. Phys. Solids, **7**, p. 209.
[21] Hill, R., 1950, *The Mathematical Theory of Plasticity*, Oxford University Press, Oxford, UK.
[22] Rudnicki, J. W., 1977, *The Effects of Stress-Induced Anisotropy on a Model of Brittle Rock Failure as Localization of Deformation*, Energy Resources and Excavation Technology, Proc. 18th US symposium on Rock Mechanics, Keystone, CO, June 22–24, pp. 3B4.1–8.
[23] Chau, K. T., 1995, ''Buckling, Barelling, and Surface Instabilities of a Finite, Transversely Isotropic Circular Cylinder,'' Q. J. Mech. Appl. Math., **53**(2), pp. 225–244.